Chapter 3
Aerobic oxidation of DNA with non-heme iron complexes

Non-heme iron(II) complexes have been used in the aerobic oxidation of DNA. In this chapter, a study of the DNA cleaving properties of the complex iron(II) N4Py and a derivative with a covalently attached DNA intercalator is described. The covalent attachment of acridine (DNA intercalator) resulted in a fourfold increase in the rate of the oxidation of DNA. However, both complexes oxidized DNA via the same pathway, with only single strand cleavage activity observed. The addition of mechanistic probes pointed towards the involvement of reduced oxygen species (in particular superoxide) as key intermediates in the hydrogen abstraction process, ultimately resulting in DNA strand breaks.

3.1 Introduction

In Chapter 1, an overview of DNA cleavage and the mechanistic insights that can be gained from studying the catalytic activity was presented.[1] The focus of this chapter is on the oxidative cleavage of DNA, *i.e.* the induction of strand cuts in DNA, via an oxidative mechanism. One of the most prominent and famous examples of an oxidative DNA cleavage agent is bleomycin (or iron bleomycin). Its application as an effective chemotherapeutic agent against cancer,[2-7] and its fascinating, although still not fully understood, chemistry,[8-14] has led bleomycin to serve as an inspiration for many artificial oxidative DNA cleavage agents, both in terms of activity and structure.[15-21]

3.1.1 DNA cleavage with Fe(N4Py) complexes

The pentadentate ligand N4Py was developed in a combined effort between our group and the research group of Prof. L. Que, Jr.[22,23] By complexation of this ligand to iron(II) in acetonitrile, the stable low spin iron(II) complex $[Fe^{II}(N4Py)(CH_3CN)]^{2+}$ (**1**) was obtained (Figure 3.1, left). Treatment of $[Fe^{II}(N4Py)(CH_3CN)]^{2+}$ with peroxides gave rise to a range of interesting intermediates, including $[(N4Py)Fe^{III}OOH]^{2+}$,[23] and $[(N4Py)Fe^{IV}{=}O]^{2+}$.[24]

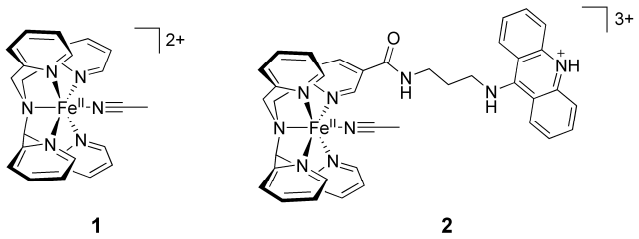

Figure 3.1 Complexes examined in this study, $[(N4Py)Fe^{II}(CH_3CN)]^{2+}$ (**1**) and $[(N4Py\text{-acridine})Fe^{II}(CH_3CN)]^{3+}$ (**2**).

Initial work demonstrated that **1** is capable of inducing DNA strand breaks, even in the absence of a sacrificial reductant.[25] The addition of **1** (10 μM final concentration) to supercoiled Litmus29 plasmid DNA (2820 base pairs, ratio iron complex : DNA base pairs, ~ 1:15) resulted in instant activity. This could be concluded from the fact that nicked DNA was formed almost immediately, *i.e.* within approximately 30 s, taking into account the time required for addition and quenching (Figure 3.2, lane 2). This initial burst of activity was followed by a slow build up of nicked DNA over a period of several hours, indicating that **1** remained active in inducing DNA strand cuts.[25]

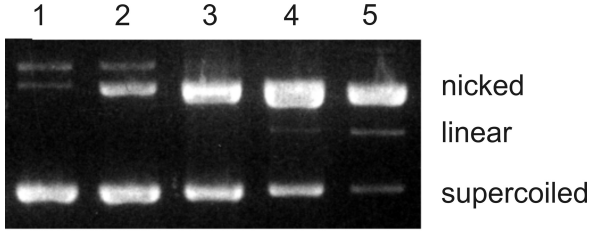

Figure 3.2 Aerobic oxidation of Litmus29 plasmid DNA catalyzed by $[Fe^{II}(N4Py)(CH_3CN)](ClO_4)_2$ (**1**) (10 μM) without additional reductant followed in time. Lane 1, control; lane 2, t = 0; lane 3, t = 1 h; lane 4, t = 4.5 h; lane 5, t = 18 h. Adapted with permission from 25; copyright 2000, J.G. Roelfes.

The design principles of bleomycin (BLM)[26] and methidiumpropyl EDTA (MPE)[27] were followed by the covalent attachment of an DNA intercalator to further increase the DNA cleaving activity of **1**. Acridine was chosen for this purpose because of its high DNA binding constant[28] and negligible sequence specificity.[29] The introduction of a functional group at the 5-position of one of the pyridines of the N4Py scaffold allowed for the covalent attachment of a small flexible spacer to which the acridine could be bound. The resulting N4Py ligand with the acridine bound peripherally, was coordinated to iron(II) and the resulting complex **2** (Figure 3.1, right) displayed DNA cleavage activity already at concentrations as low as 100 nM in the presence of an additional reductant (dithiothreitol (DTT) or ascorbic acid).[25]

This complex **2** is also capable of inducing DNA strand cuts at a 1.0 μM concentration (ratio iron complex : base pairs, ~ 1:150) *without* the presence of an additional reductant (Figure 3.3, lane 3). Moreover, the aforementioned burst of activity was observed again.[30] This instant activity at these low concentrations has only been observed with [Fe(BLM)] (Figure 3.3, lane 6) and more recently with a pentapyridyl iron(II) complex.[31]

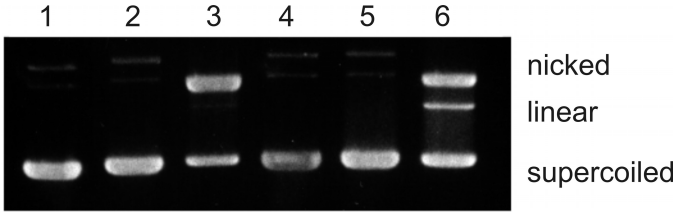

Figure 3.3 Gel of DNA cleavage with various complexes at 1.0 μM concentration without additional reductant after ~ 30 sec. Lane 1, control; lane 2, $[Fe^{II}(N4Py)(CH_3CN)](ClO_4)_2$ (**1**); lane 3, $[Fe^{II}(N4Py\text{-acridine})(CH_3CN)](ClO_4)_3$ (**2**); lane 4, Fe(N4Py) complex without the acridine bound to the spacer; lane 5, Fe(MPE); lane 6, Fe(BLM). Adapted with permission from 25; copyright 2000, J.G. Roelfes.

The reaction of **2** with DNA results in two distinguishable cleavage products; the 3'-phosphate and 3'-phosphoglycolate, which match with products found using Fe(BLM)[32] and Fe(MPE) (Figure 3.4).[33] The formation of the 3'-phosphoglycolate product points towards hydrogen abstraction at the C4' position, which is located in the minor groove. The 3'-phosphate product indicates that other mechanisms are involved also (*e.g.* C1' and C3' hydrogen abstraction).[32] Importantly, a hydrolytic mechanism can be excluded,[34-37] as the restriction fragments of DNAse do not correspond to the cleavage products observed with **2**.[25,30]

3.1.2 Outline of this chapter

The initial work on **1** and **2** showed that these complexes are highly reactive towards the oxidation of DNA. The first part of this chapter focuses on the kinetics and cleavage chemistry, displayed by the iron N4Py complexes **1** and **2**. By making use of the methods and analyses introduced in Chapter 2, the cleavage pathway, *i.e.* a single strand or a double strand cleavage pathway, can be distinguished.

At the start of this investigation, no information was available about the nature of the reactive species that performs the actual hydrogen abstraction in the DNA backbone. This process was examined by using a combination of mechanistic probes, such as DMSO, superoxide dismutase (SOD) and catalase, and spectroscopy. Based on the data obtained, a hypothesis with regard to the nature of the oxidizing species can be formulated.

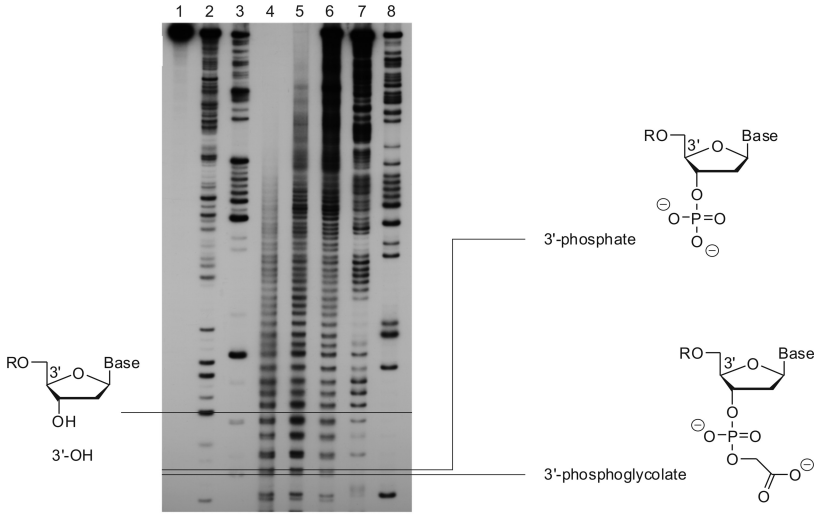

Figure 3.4 High resolution denaturing PAGE gel of cleavage products of a 5'-^{32}P-end labeled 172 base pair restriction fragment after 1 h reaction. Cleavage reactions performed in Tris buffer (10 mM, pH 8.0) at 37 °C in the presence of 1 mM DTT. Lane 1, control; lane 2, DNaseI; lane 3, Fe(BLM) (10 μM); lane 4, Fe(MPE) (10 μM); lane 5, [Fe^{II}(N4Py-acridine)(CH_3CN)](ClO_4)$_3$ (**2**) (10 μM); lane 6, [Fe^{II}(N4Py-acridine)(CH_3CN)](ClO_4)$_3$ (**2**) (1 μM); lane 7, C & T; lane 8, G. Adapted with permission from 25; copyright 2000, J.G. Roelfes.

3.2 Aerobic DNA oxidation

The DNA oxidation reactions were performed at 37°C and the solutions were buffered to ascertain a constant pH. The buffer used was set at pH = 8.0, which approximates the basicity under physiological conditions at 37°C. Three buffers were tested for their suitability in the DNA oxidation reaction, namely a tris(hydroxymethyl)aminomethane (Tris) buffer, a phosphate buffer, and a 2-[4-(2-hydroxyethyl)-1-piperazine]ethanesulfonic acid (HEPES) buffer. Complex **1** (1.0 μM, final concentration) was added to the buffered solution (10 mM, final concentration, pH 8.0) of supercoiled pUC18 plasmid DNA (2686 base pairs, 0.1 μg/μl, 150 μM, final concentration) and the reaction mixture was incubated at 37°C. After 30 min, the reaction mixture was sampled and quenched with a solution of dye number IV (See Chapter 2) and 1000 equivalents of NaCN to ascertain a complete quenching. Addition of an excess of NaCN ensures complete quenching of the reaction, as this gives rise to the formation of the catalytically inactive $Fe^{II}(CN)_6$ complex. The efficiency of quenching has been confirmed by the absence of activity when: i) $(NH_4)_4Fe^{II}(CN)_6$ was employed as catalyst and ii) NaCN (1000 eq) was added to the DNA reaction mixture together with **1**.

Usage of a Tris buffer leads to a near complete conversion of the initial supercoiled DNA into the nicked DNA in 30 min (Figure 3.5, lane 1). In contrast, when a phosphate buffer was used in place of a Tris buffer at the same pH, a clear reduction in activity was observed, as a significant amount of supercoiled DNA was still present after 30 min (Figure 3.5, lane 2). Presumably, this reduction in activity is the result of a direct interaction between **1** and phosphate.[38] The cleavage results with a HEPES buffer are comparable to

that of the Tris buffer (Figure 3.5, lane 3). Based on these results, further reactions were performed in Tris buffer.

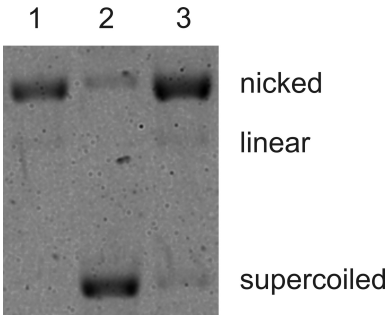

Figure 3.5 Oxidation of supercoiled pUC18 plasmid DNA (0.1 μg/μL; 150 μM in bp) by $[Fe^{II}(N4Py)(CH_3CN)](ClO_4)_2$ (**1**) (1.0 μM) in the presence of DTT (1.0 mM) in different buffers (10 mM) at pH 8.0 after 30 min. Lane 1, Tris buffer; lane 2, phosphate buffer; lane 3, HEPES buffer. The figure is representative for a triplicate experiment.

Due to the high activity of Fe(N4Py-acridine) (**2**), it was investigated whether this complex could be used at lower concentrations. A titration experiment showed activity that was observed at concentrations as low as 5 nM, which corresponds to an iron to base pair ratio of 1:30.000 and makes this complex still one of the most active complexes for DNA cleavage reported to date (Figure 3.6).

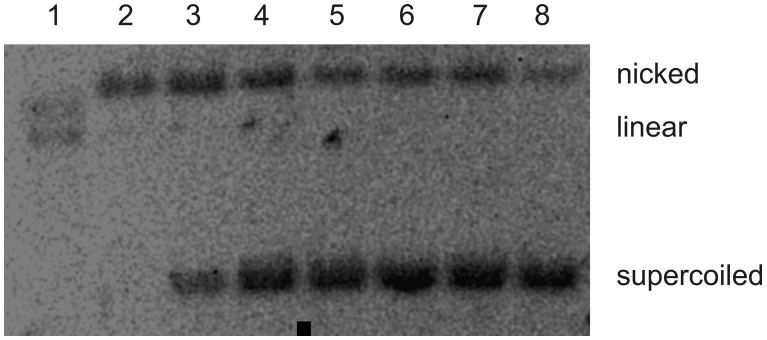

Figure 3.6 Oxidation of supercoiled pUC18 plasmid DNA (0.1 μg/μL; 150 μM in bp) in Tris buffer (10 mM) in the presence of DTT (1.0 mM) and $[Fe^{II}(N4Py\text{-}acridine)(CH_3CN)](ClO_4)_3$ (**2**) in various concentrations after 60 min. Lane 1, 1.0 μM; lane 2, 0.10 μM; lane 3, 50 nM; lane 4, 25 nM; lane 5, 12.5 nM; lane 6 10 nM; lane 7, 5.0 nM; lane 8, blank (no catalyst added).

3.2.1 DNA oxidation followed in time

The time course of the reaction of supercoiled DNA with **1** and **2** was examined (Figure 3.7), under the aforementioned conditions (*i.e.* 0.1 μg/μl; 150 μM in bp pUC18 plasmid DNA, 10 mM Tris buffer (pH 8.0) and 1.0 μM complex at 37°C). Although the complexes **1** and **2** are active in DNA cleavage without additional reductant,[25,30] in this study a reductant was added (DTT, 1.0 mM, final concentration) to facilitate comparison of activity of the complexes.

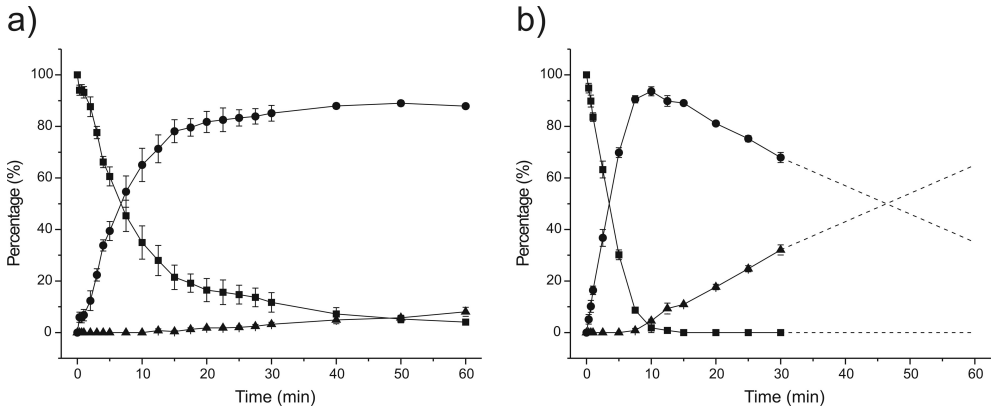

Figure 3.7 Aerobic oxidation of supercoiled plasmid DNA (■) into nicked DNA (●) and linear DNA (▲) followed in time catalyzed by a) $[Fe^{II}(N4Py)(CH_3CN)](ClO_4)_2$ (**1**) and b) $[Fe^{II}(N4Py\text{-acridine})(CH_3CN)](ClO_4)_3$ (**2**). Errors bars represent the root mean square (rms) error based on three runs. A correction factor of 1.31 was used to compensate for the reduced ethidium bromide uptake capacity of supercoiled DNA (see Chapter 2). Data obtained after 30 min for **2** is not reliable due to fragmentation of the linear DNA to smaller fragments due to extensive cleavage activity (dashed line).

Complex **1** converts supercoiled DNA into nicked DNA ($t_{1/2}$ ~ 10 min), and into linear DNA in the course of the reaction (Figure 3.7a). The covalent attachment of acridine (complex **2**) has a profound influence on the reaction rate; nicked DNA is produced at a much higher rate ($t_{1/2}$ ~ 5 min) (Figure 3.7b). Moreover, nearly all supercoiled DNA is consumed after 10 min and already significant amounts of linear DNA are observed at that time. After 10 min, the amount of nicked DNA decreases and is accompanied with a steady increase in the amount of linear DNA. After 30 min, around 30% of linear DNA is formed, which is the maximum amount, which can be quantified accurately (see Chapter 2). Data obtained at later stages of the reaction are unreliable, as the linear DNA is oxidized into smaller fragments, resulting in the appearance of a smear on the agarose gel.

3.2.2 Single strand *vs.* double strand cleavage pathway

On initial inspection, it would appear that the linear DNA is formed as a result of extensive single strand cleavage, both with **1** or **2** as catalyst. The linear DNA is produced, when all supercoiled DNA is converted into nicked DNA, which is typical for a single strand cleavage agent. To verify that both **1** and **2** are indeed typical single strand cleavage agents, the average number of single (n) and double strand cuts (m) in a DNA molecule can be calculated using both Equation 3.1 and Equation 3.2 (see Chapter 2 for details).[39] The data obtained can be compared to a theoretical maximum of linear DNA, which is to be expected from extensive single strand cleavage activity (Freifelder-Trumbo relation, Equation 3.3).[40] The results are presented in Figure 3.8.

$$f_{III} = m \times e^{-m}$$

Equation 3.1 Average number of double strand cuts in one DNA molecule, calculated from the fraction of linear DNA (f_{III}).

$$f_I = e^{-(m+n)}$$

Equation 3.2 The total number of strand cuts (both single (*n*) and double (*m*)) in one DNA molecule calculated from the remaining fraction of DNA without any cuts.

$$m = \frac{n^2(2h+1)}{4L}$$

Equation 3.3 The Freifelder-Trumbo relationship, with *h* as the maximum distance in base pairs between nicks on opposite strands to generate a double strand cut (*i.e.* 16)[40] and *L* the total number of base pairs of the DNA used (2686 base pairs for pUC18 plasmid DNA).

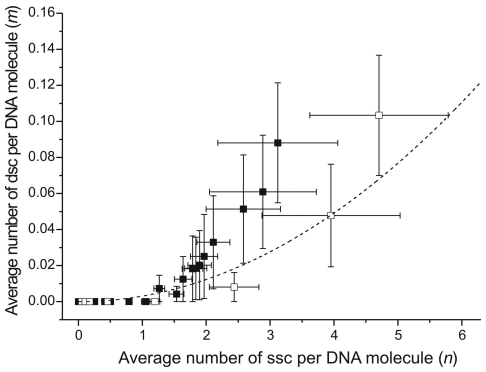

Figure 3.8 Number of double strand cuts (dsc, *m*) per DNA molecule plotted as a function of the number of single strand cuts (ssc, *n*) per DNA molecule for both **1** (■) and **2** (□).The dotted line is the Freifelder-Trumbo relation (Equation 3.3).[40] Error bars represent the uncertainty limits of the data, based on a Monte Carlo simulation, taking into account a standard deviation σ of 0.03 of the individual DNA fractions.

When a (mathematical) function is applied to calculate values from experimental data, the errors in these experimental data have an effect on the final outcome. Normally, when the error in *x* is equal to σ_x, the expected error in σ_f in $f(x)$ will be equal to of the function by differentiation of the function (Equation 3.4).[41]

$$\sigma_f = \left|\frac{df}{dx}\right|\sigma_x$$

Equation 3.4 Expected error in the function *f* from the error in *x*, where σ_x is the error in *x* and σ_f is the expected error in $f(x)$.

The calculation of the errors or uncertainties in the values of both *n* and *m* using Equation 3.1 and Equation 3.2, will lead to difficult mathematical problems. The experimental error in the fraction of linear DNA will cause an error in the value of *m*. This error in *m* should be taken into account when *n* is calculated in Equation 3.2. However, the experimental error in the fraction of supercoiled DNA influences the error of *n* also. Moreover, it should be taken into account that the sum of all three fractions of DNA is always equal to 1. Due to this mathematical complexity, it was decided to use a so-called Monte Carlo simulation method to calculate the uncertainty limits of both *n* and *m*.

This Monte Carlo simulation calculates the uncertainty of the values of *n* and *m*, by generation of pseudo-random fractions of supercoiled, nicked and linear DNA based on the average value within a standard deviation of 0.03. This standard deviation for the fractions of different types of DNA was determined by repeating an oxidation experiment of supercoiled DNA with **1** (1.0 μM) and DTT (1.0 mM) 24 times, with quenching at t = 30 min. These obtained pseudo-random fractions (which obey the requirement that the sum of the three fractions should always be equal to 1) were used to calculate the outcomes of *n* and *m*. In this way, a good measure was obtained for the spread of the values of *n* and *m*.

The behavior of complexes **1** and **2** is quite similar in terms of the type of DNA cleavage pathway. Initially, only formation of nicked DNA is observed, indicating that only single strand cuts are introduced in the DNA. Only after some time, linear DNA is formed also, which is the result of double strand DNA cuts (Figure 3.7). This trend for both complexes is reflected in Figure 3.8, as the calculated average number of double strand cuts per DNA molecule (*m*) only increases when a significant number of single strand cuts per DNA molecule (*n*) is present. The obtained values of *n* and *m* approximate the line of the Freifelder-Trumbo relationship (Equation 3.3), which predicts the number of double strand cuts to be expected from extensive single strand DNA cleavage. Therefore, these experiments demonstrate that both **1** and **2** are single strand cleavage agents and that direct double strand cleavage is not achieved with these complexes.

3.2.3 Rate of the reaction

Since both complexes **1** and **2** only induce single strand breaks, the average number of strand cuts per DNA molecule can be calculated, taking into account that the formation of linear DNA is the results of two independent single strand cleavage events by using Equation 3.5 (when no linear DNA is present) and Equation 3.6 (when linear DNA is present, see Chapter 2 for details).

$$f_I = e^{-n}$$

Equation 3.5 Average number of single strand cuts (*n*) in a DNA molecule, calculated from the fraction of supercoiled DNA (f_I).

$$f_I + f_{II} = \left[1 - n(2h+1)/2L\right]^{n/2}$$

Equation 3.6 Average number of single strand cuts (*n*) in a DNA molecule, calculated from the fractions supercoiled (f_I) and nicked (f_{II}) DNA. This equation takes the maximum distance in base pairs between nicks on opposite strands to generate a double strand cut (*i.e.* 16 base pairs)[40] (*h*) and the total number of base pairs of the DNA used (*L*).

In order to determine the order of the reaction, different concentrations of DTT were employed (Figure 3.9). Without DTT as a reductant, around 20% nicked DNA is formed after 30 min (Figure 3.9a, lane 1). This corresponds to 0.25 (± 0.03) single strand cuts per DNA molecule, calculated with Equation 3.5 (Figure 3.9b). With an equimolar concentration of DTT with respect to **1** (final concentration of 1.0 μM) around three times as much nicked DNA is formed in the same period (*ca.* 60%, Figure 3.9a, lane 2), which corresponds to 0.92 (± 0.06) single strand cuts per DNA molecule (Figure 3.9b). Higher concentrations of DTT (ranging from 10 μM to 1.0 mM) resulted in a dramatic increase in the reaction rate, as the number of single strand cuts per DNA molecule increased by a factor of six, calculated with Equation 3.6 (Figure 3.9b). Since the reaction is performed at

a final concentration of 1.0 mM DTT, the reaction under these conditions can be considered as a pseudo-first order reaction.[42,43]

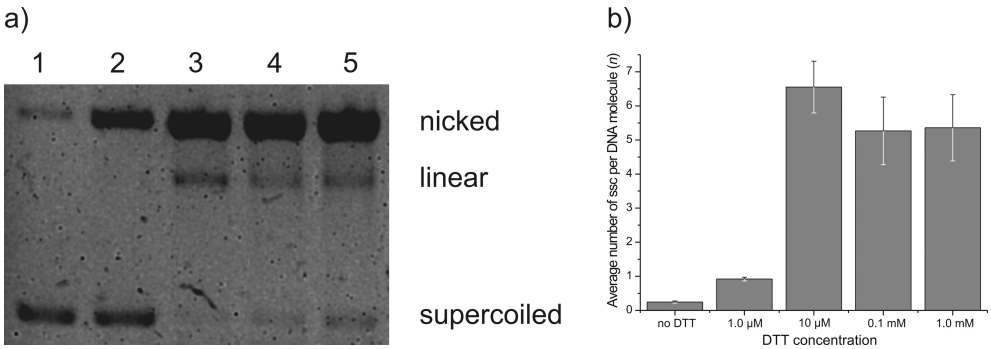

Figure 3.9 Oxidation of supercoiled pUC18 plasmid DNA (0.1 µg/µL; 150 µM in bp) in Tris buffer (10 mM) in the presence of **1** (1.0 µM) and various concentrations of DTT after 30 min. a) Agarose gel after 30 min. Lane 1, no DTT; lane 2, 1.0 µM DTT; lane 3, 10 µM DTT; lane 4, 100 µM DTT; lane 5, 1.0 mM DTT. b) Calculated average number of single strand cuts (ssc) per DNA molecule with different concentrations of DTT. Error bars represent the uncertainty limits of the data, based on a Monte Carlo simulation, taking into account a standard deviation σ of 0.03 of the individual DNA fractions.

Based on a pseudo-first order reaction, the decrease in the concentration of supercoiled DNA in time can be used to calculate k_{obs}. When the natural logarithm of f_I is plotted as a function of time, k_{obs} can be determined from the slope of the linear fit (Figure 3.10).[42,43] From these data k_{obs} for **1** was calculated to be ~ 0.1 min^{-1}. Unfortunately, the data for **2** did not allow a reliable estimation of k_{obs}. Due to a faster DNA cleavage process with **2** compared to **1**, the fraction of supercoiled DNA is small, which leads to large uncertainties in the data (the error σ is equal to $\sigma_{[DNA]}$/[DNA], Equation 3.4). Use of the fraction of the nicked DNA suffers from the same problem, as the fraction of nicked DNA is small initially.

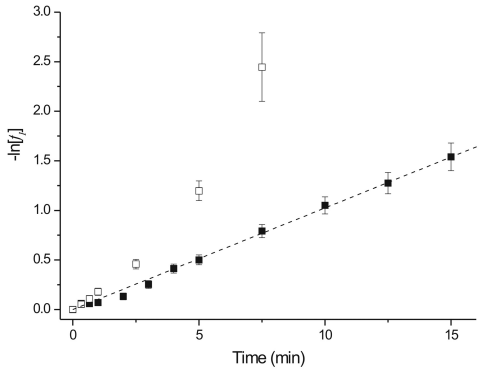

Figure 3.10 -Ln[f_I] plotted as a function of time for **1** (■) and **2** (□). The dashed line is a linear fit of the data obtained using **1** (k_{obs} = 0.103 +/- 0.002, R^2 = 0.997). Error bars represent the expected deviation, based on a standard deviation σ of 0.03 in the fraction of supercoiled DNA (f_I).[41]

An alternative approach to the use of the fraction of supercoiled DNA for the kinetic analysis is by using the number of single strand cuts per DNA molecule at the present DNA concentration. The average number of single strand cuts per DNA molecule can be calculated for **1** and **2** at each time point, by using Equation 3.5 and Equation 3.6. The result can be plotted as a function of time (Figure 3.11). It should be noted, that whenever linear DNA is present (especially when small amounts are present) and Equation 3.6 is used to calculate the number of strand cuts, relatively large error margins are observed. This is due to the fact that small deviations in the amount of linear DNA results in large differences in the results obtained from Equation 3.6. The data presented in Figure 3.11 show the difference in activity in DNA oxidation between **1** and **2**. The rate constant of single strand DNA cleavage of $[Fe(N4Py)(CH_3CN)]^{2+}$ (**1**) determined from the slope of the graph is 0.095 ± 0.003 min^{-1}, which corresponds well to the value reported previously (k_{obs} = 0.103 ± 0.002, Figure 3.10). Complex **2** with the covalently attached acridine shows a fourfold increase in the rate constant (0.379 ± 0.011 min^{-1}), demonstrating the positive influence of this DNA intercalating moiety. The linear relation between the concentration of single strand cuts and time further demonstrate that only single strand cleavage activity is observed with the mononuclear complexes **1** and **2**. Moreover, by calculating the concentration of single strand cuts, the reaction constant of **2** could be determined. In this respect, this approach is ideal for very active single strand DNA cleavage agents, as more data points can be taken into consideration to calculate this rate constant. Active DNA cleavage complexes will result in a fast decrease in the fraction of supercoiled DNA. This lead to relative large error margins, complicating the determination of the rate via the 'classical' method (*vide supra*).

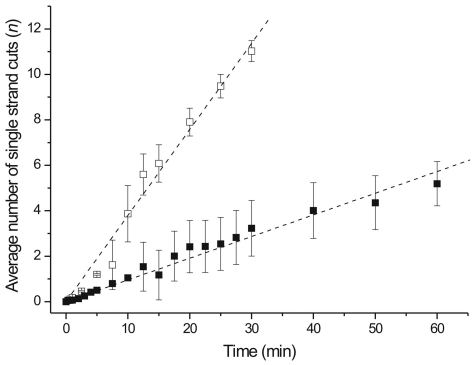

Figure 3.11 Average number of single strand cuts per DNA molecule as a function of time for **1** (■) and **2** (□). Dashed lines represent the linear fit through the data points for **1** (0.095 ± 0.003 min^{-1}, R^2 = 0.976) and **2** (0.379 ± 0.011 min^{-1}, R^2 = 0.984). Error bars represent the uncertainty limits of the data, based on a Monte Carlo simulation, taking into account a standard deviation σ of 0.03 of the individual DNA fractions.

The turnover frequency (TOF, *i.e.* turnover number (TON) per second) of single strand cuts for **1** and **2** are 0.32 $s^{-1}$and 1.30 s^{-1}, respectively. These data demonstrate unequivocally that the system is catalytic in terms of inducing strand cuts in the DNA. Unfortunately, it is difficult to compare the results for **1** and **2** with results obtained with other complexes, which have been used as single strand cleavage agents. This is due to the fact that often different conditions (such as pH and temperature) are used, which makes it impossible to compare the data reliably. Moreover, often the data obtained are not corrected for the

reduced ethidium bromide uptake of supercoiled DNA, which can account for errors up to 20-30% in the final results.

3.3 Nature of the active species

An important question is what the actual hydrogen abstracting species during DNA oxidation is. Recent progress on the mechanism of BLM-based DNA oxidation indicates that the hydrogen abstracting species are metal bound intermediates ((BLM)Fe^{III}OOH and (BLM)Fe^{IV}=O).[44] On the other hand, reduced oxygen species (hydroxyl radicals) are responsible for DNA cleavage induced by the $[Fe(EDTA)]^{2-}/H_2O_2$/ascorbate system, instead of high-valent iron intermediates.[45] In this paragraph the possibility for involvement of both mechanisms in the hydrogen abstracting process induced by **1** are examined and discussed.

3.3.1 Reactive oxygen species scavengers

A readily accessible and experimentally facile method for the examination of the reaction under catalytic conditions is via the use of mechanistic probes. These probes can provide insight into whether reduced oxygen species (ROS), such as superoxide, hydrogen peroxide or hydroxyl radicals, are present during the reaction. The most commonly used reactive oxygen species scavengers are superoxide dismutase (SOD, an enzyme, which converts superoxide radicals into dioxygen and hydrogen peroxide)[46-51] and catalase (which converts hydrogen peroxide into dioxygen and water).[52-54] The effect of the addition of hydrogen peroxide was investigated also. Finally, dimethyl sulphoxide (DMSO), was used as a hydroxyl radical scavenger.[55]

The additives SOD, catalase, DMSO or a combination of SOD and catalase were added to the reaction mixture prior to the addition of the complex (and the reductant) and the reactions were quenched after 30 min, identically as described earlier (*vide supra*). After analysis by gel electrophoresis, the obtained fractions of supercoiled, nicked and linear were used to calculate the average number of single strand cuts per DNA molecule. A reliable quantification of the influence of different scavengers and additives can be obtained with Equation 3.5 and Equation 3.6.

3.3.1.1 Enzymatic ROS scavengers in DNA oxidation in the absence of DTT

First, the reaction was examined in the absence of a reductant (DTT), using dioxygen as terminal oxidant (*vide supra*). The overall activity was much lower than when a reductant is used (*cf.* Figure 3.12a, lane 1 and Figure 3.14a, lane 1 (*vide infra*)); only 25% nicked DNA was formed after 30 min. The addition of SOD caused a slight drop in activity (Figure 3.12a, lane 2), whereas the presence of catalase did not affect the reaction outcome (Figure 3.12a, lane 3). A more pronounced inhibition is observed when both enzymes are added to the reaction (Figure 3.12a, lane 4).

The degree of inhibition by the enzymes can be quantified by calculating the average number of single strand cuts per DNA molecule (Figure 3.12b). The addition of SOD results in ~ 40% inhibition, and in combination with catalase an even higher degree of inhibition was obtained (up to 70%). This result suggests a cooperative inhibition of these two enzymes, as catalase alone did not influence the reaction.

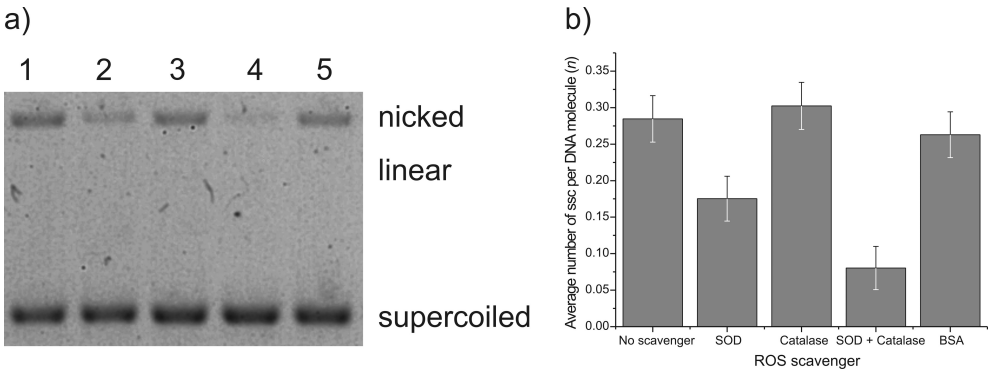

Figure 3.12 Comparison of the oxidative DNA cleavage efficiency of **1** without additional reductant in the presence of enzymatic ROS scavengers at T = 30 min. a) Agarose gel after 30 min. Lane 1, no ROS scavenger; lane 2, SOD (1.0-5.0 U); lane 3, catalase (1.0-2.5 U); lane 4, SOD (1.0-5.0 U) and catalase (1.0-2.5 U); lane 5, BSA (1 μg). b) Calculated average number of single strand cuts (ssc) per DNA molecule in the presence or absence of ROS scavengers. Error bars represent the uncertainty limits of the data, based on a Monte Carlo simulation, taking into account a standard deviation σ of 0.03 of the individual DNA fractions.

When hydrogen peroxide was used in the reaction as terminal oxidant instead of dioxygen, a dramatic increase in nicked DNA was observed after 30 min. Moreover, the overall activity was comparable to that of O_2/DTT (*cf.* Figure 3.13a, lane 1 and Figure 3.14a, lane 1, (*vide infra*)). The addition of catalase inhibits the reaction significantly (Figure 3.13a, lanes 3 and 4), which is the result of the disproportionation of hydrogen peroxide into water and dioxygen by this enzyme. Surprisingly, SOD inhibits the reaction (Figure 3.13a, lane 2) also, by ~ 75% (Figure 3.13b). This overall inhibition pattern is comparable to the inhibition pattern, displayed by many other non-heme iron complexes systems, such as $[Fe^{III}(MPE)]$,[27] $[Fe^{III}(BDPEA)(Cl)_2]$,[56] and $[Fe^{II}(L_5^+)(Cl)]$.[57]

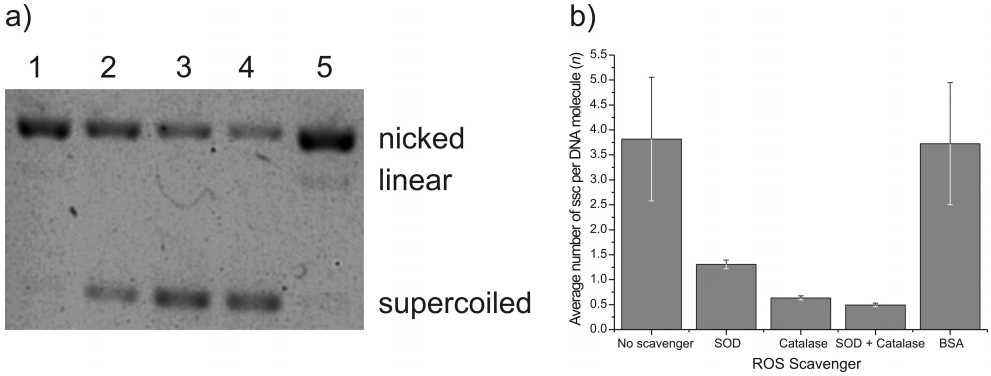

Figure 3.13 Comparison of the oxidative DNA cleavage efficiency of **1** with H_2O_2 in the presence of enzymatic reactive oxygen species (ROS) scavengers at T = 30 min. a) Agarose gel after 30 min. Lane 1, no ROS scavenger; lane 2, SOD (1.0-5.0 U); lane 3, catalase (1.0-2.5 U); lane 4, SOD (1.0-5.0 U) and catalase (1.0-2.5 U); lane 5, BSA (1 μg). b) Calculated average number of single strand cuts (ssc) per DNA molecule in the presence or absence of ROS scavengers. Error bars represent the uncertainty limits of the data, based on a Monte Carlo simulation, taking into account a standard deviation σ of 0.03 of the individual DNA fractions.

3.3.1.2 Enzymatic ROS scavengers in DNA oxidation in the presence of DTT

When DTT was added to the reaction, a significant increase in the reaction rate is observed compared to conditions without reductant (*cf.* Figure 3.12 and Figure 3.14). DTT is thought to reduce an inactive iron(III) complex back to an active iron(II) complex, which then reacts again with dioxygen. Under these conditions, a completely different behavior was observed with the enzymatic additives. The addition of SOD increased the overall reaction by a factor of two (Figure 3.14b). This suggests the involvement of superoxide radicals, as SOD converts these intermediates promptly into hydrogen peroxide, which then can react further as oxidant. The formation of hydrogen peroxide by SOD is further substantiated by the drop in the overall activity upon addition of catalase (Figure 3.14a, lane 4 and Figure 3.14b).

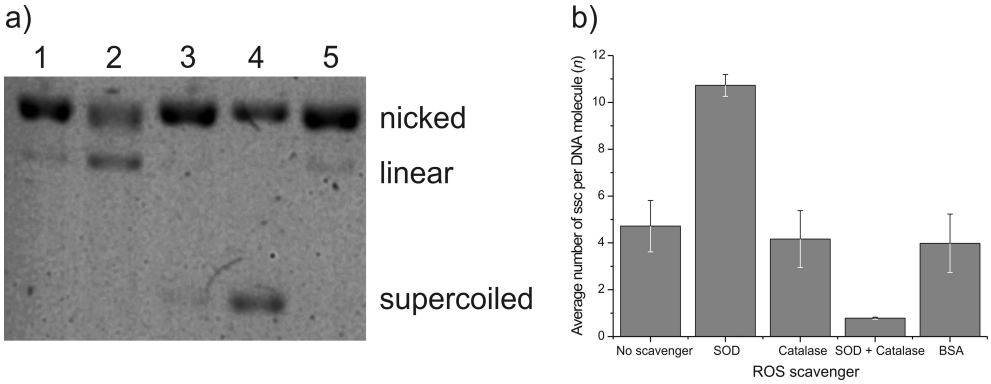

Figure 3.14 Comparison of the oxidative DNA cleavage efficiency of **1** with DTT in the presence of enzymatic reactive oxygen species (ROS) scavengers at T = 30 min. a) Agarose gel after 30 min. Lane 1, no ROS scavenger; lane 2, SOD (1.0-5.0 U); lane 3, catalase (1.0-2.5 U); lane 4, SOD (1.0-5.0 U) and catalase (1.0-2.5 U); lane 5, BSA (1 μg). b) Calculated average number of single strand cuts (ssc) per DNA molecule in the presence or absence of ROS scavengers. Error bars represent the uncertainty limits of the data, based on a Monte Carlo simulation, taking into account a standard deviation σ of 0.03 of the individual DNA fractions.

An even higher cleavage activity was observed when H_2O_2 was added (Figure 3.15). Unfortunately, due to this high rate, the fractions of nicked and linear DNA observed do not allow a reliable quantification of the data, due to extensive strand cleavage activity. However, from a qualitative perspective, it can be concluded that the presence of catalase generally inhibits the reaction, whereas SOD causes an increase in strand cleavage activity. Indeed, an increased DNA cleavage activity with hydrogen peroxide (generated *in situ* by SOD) in the presence of DTT has been observed with the O_2/DTT system (Figure 3.14).

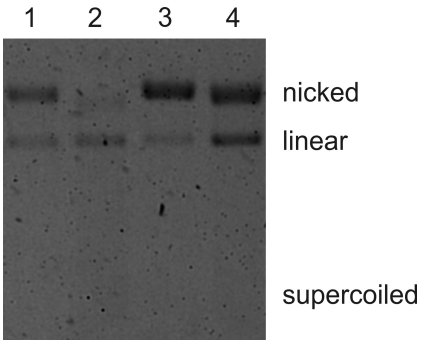

Figure 3.15 Agarose gel of DNA oxidation with **1** (1.0 μM), H_2O_2 (1.0 mM) and DTT (1.0 mM) after 30 min. Lane 1, no ROS scavenger; lane 2, SOD (1.0-5.0 U); lane 3, catalase (1.0-2.5 U); lane 4, SOD (1.0-5.0 U) and catalase (1.0-2.5 U).

The presence of protein in the reaction mixture does not have a negative effect on the reactions. As a control, bovine serum albumin (BSA, 1.0 μg, which corresponds approximately to the amount of SOD or catalase added to the reaction) was added to the reaction. No significant difference in the reaction outcomes was observed by the addition of this protein (Figure 3.12, Figure 3.13, and Figure 3.14).

3.3.1.3 Oxidation of DNA in the presence of DMSO

A well-established method to induce single strand cleavage in DNA is via reaction with highly reactive hydroxyl radicals, which can react at various positions in the DNA strand to form alkali labile sites or induce direct strand cleavage.[32,58] These hydroxyl radicals can be generated via irradiation of water with γ-rays,[59] or via Fenton chemistry (iron(II) salt and H_2O_2).[60] The addition of DMSO to this reaction mixture inhibits the hydroxyl radical mediated DNA cleavage process, by 80%, due to reaction between DMSO and the hydroxyl radicals.[55]

When **1** was employed as catalyst, under all aforementioned conditions no significant influence of the cleavage activity was observed when DMSO was added (Figure 3.16). Therefore, the role of hydroxyl radicals in the reaction mechanism are of less importance and thus do not contribute significantly to the hydrogen abstraction process.

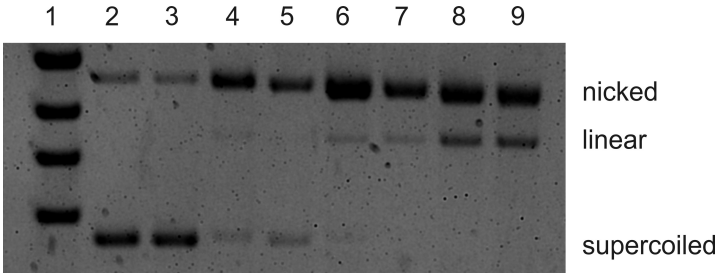

Figure 3.16 Agrose gel of aerobic DNA oxidation with **1** in the presence of absence of DMSO after 30 min. Lane 1, DNA ladder; lane 2, **1** (1.0 μM); lane 3, **1** (1.0 μM) and DMSO (1.0 mM); lane 4, **1** (1.0 μM) and DTT (1.0 mM); lane 5, **1** (1.0 μM), DTT (1.0 mM), and DMSO (1.0 mM); lane 6, **1** (1.0 μM) and H_2O_2 (1.0 mM); lane 7, **1** (1.0 μM), H_2O_2 (1.0 mM), and DMSO (1.0 mM); lane 8, **1** (1.0 μM), DTT (1.0 mM), and H_2O_2 (1.0 mM); lane 9, **1** (1.0 μM), DTT (1.0 mM), H_2O_2 (1.0 mM), and DMSO (1.0 mM).

3.3.1.4 Discussion of DNA oxidation in the presence of ROS scavengers

From the results presented here, it appears that superoxide plays a crucial role in the reaction mechanism of hydrogen abstraction from DNA catalyzed by **1**. When DTT is employed as an additional reductant, the presence of SOD significantly increases the reaction rate by the formation of hydrogen peroxide from superoxide (Figure 3.14). This has been confirmed by the independent addition of hydrogen peroxide to the **1**/O_2/DTT system (Figure 3.15). Moreover, the addition of SOD in combination with catalase suppresses the reaction significantly, which indeed indicates that hydrogen peroxide is formed by SOD. The presence of 'free' hydroxyl radicals was excluded; inhibition was not observed when DMSO was added to the reaction mixture.

So can superoxide be the actual hydrogen abstracting species in solution, resulting in DNA strand breaks? Up to now, no definitive evidence has been published to support this hypothesis. However, it has been demonstrated that DNA strand cleavage induced by KO_2 under physiological conditions is the result of the autocatalytic dismutation of superoxide into hydrogen peroxide, which can act as the terminal oxidant together with a metal ion.[61] Examples of direct hydrogen abstraction by superoxide radicals from substrates with readily transferable hydrogens (such as reduced flavins, hydrophenazines and hydroxyl amines) have been published, but only in non-protic solvents, such as DMF.[62,63] Another report points towards the involvement of the conjugate acid as a hydrogen abstracting species (HO_2) rather than superoxide itself.[64] Under physiological conditions, ~ 1% of the superoxide is in the protonated form (p*K*a ~ 4.7),[65] which can engage in a hydrogen abstraction from linoleic acid (Scheme 3.1). However, the estimated rate constant for this hydrogen abstraction by HO_2 is ~ 300 $M^{-1}s^{-1}$,[64] whereas the rate constant of spontaneous decay is more than a 1000-fold higher.[65] Moreover, the reported study was performed with strict exclusion of metal ions, making it difficult to draw a parallel to the present study.

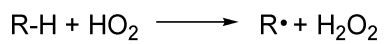

Scheme 3.1 Hydrogen abstraction from a target substrate with HO_2.

Taken together, it is unlikely that superoxide radicals are involved directly in the hydrogen abstraction from DNA. Rather, a direct interaction between the iron complex **1** and superoxide radicals is more likely. It has been demonstrated by Fee, Groves and co-workers that Fe(EDTA) can undergo a series of reactions with superoxide, in which superoxide acts both as a reductant and as an oxidant (Scheme 3.2).[66,67] Importantly, this cascade of reactions results in the formation of free hydrogen peroxide, which has been identified as an important intermediate in the degradation of DNA by Fe(MPE).[27]

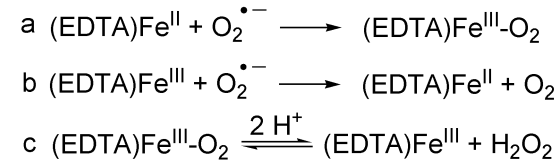

Scheme 3.2 Reaction of Fe(EDTA) complexes with superoxide radicals.

The presence of superoxide radicals has been established with **1**/O_2/DTT in DNA oxidation (Figure 3.14). This observation makes it plausible that the first step of the mechanism involves an electron transfer (either inner- or outer sphere electron transfer) of the iron(II) complex to dioxygen, resulting in an iron(III) complex, together with a superoxide radical (Scheme 3.3a). Due to the high concentration of DTT (1.0 mM) in solution, the iron(III) complex can be reduced back to an iron(II) complex (Scheme 3.3b). Alternatively, this step

can be the result of an equilibrium between an iron(III) complex and a superoxide radical (Scheme 3.3a). Interaction between the iron(II) complex and superoxide, would result in the formation of a iron(III) superoxo complex (Scheme 3.3c).

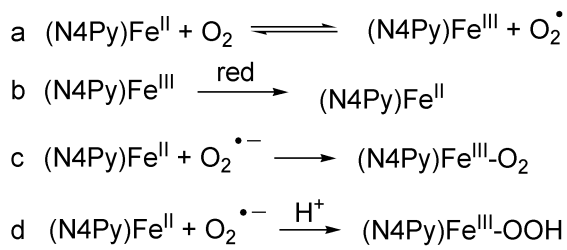

Scheme 3.3 Possible molecular oxygen activation route of **1**.

It has been demonstrated that $[(N4Py)Fe^{III}(\eta^1\text{-}OOH)]^{2+}$ can undergo a deprotonation with an appropriate base to $[(N4Py)Fe^{III}(\eta^2\text{-}O_2)]^{+}$, albeit in organic solvents.[68] In principle, this complex can be accessed via a direct reaction between superoxide and **1** (Scheme 3.3c). The resulting complex can be in equilibrium with the $[(N4Py)Fe^{III}(OOH)]^{2+}$ ('purple intermediate'), which in turn can be the terminal hydrogen abstracting species, by analogy to $[(BLM)Fe^{III}OOH]^{2+}$ ('activated bleomycin').[44] This would differ from the results with Fe(EDTA), where free hydrogen peroxide is formed, and thus the system functions as a functional model of superoxide dismutase (Scheme 3.2).

This hypothesis does not explain why the SOD influences the reaction negatively when DTT is absent (Figure 3.12, Figure 3.13). The current hypothesis requires that both $Fe^{II}(N4Py)$ (**1**) and superoxide radicals are present simultaneously (Scheme 3.3c and d). However, when no reductant is present, this probability of such an encounter is low. $Fe^{II}(N4Py)$ (**1**) reacts with dioxygen to yield $Fe^{III}(N4Py)$ together with a superoxide radical (Scheme 3.3a). The SOD converts the formed superoxide promptly into hydrogen peroxide (Scheme 3.4a). Due to the absence of a good reductant (although H_2O_2 can act as reductant as well), the probability of a successful encounter between **1** and a superoxide radical is diminished. The remaining activity could be the result of interaction between $Fe^{II}(N4Py)$ or $Fe^{III}(N4Py)$ with H_2O_2 (Scheme 3.4b). A key observation to support this hypothesis is that addition of catalase besides SOD, a further drop in activity was observed. (Figure 3.12 and Figure 3.13, lanes 4), due to the catalase catalyzed decomposition of H_2O_2 into water and molecular oxygen (Scheme 3.4c).

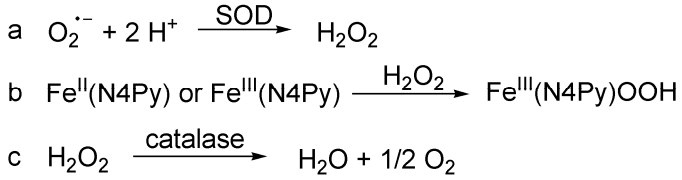

Scheme 3.4 Interaction between **1** and dioxygen, with subsequent reaction of the formed ROS with SOD and catalase.

Another hypothesis is that the inhibition by SOD is the result of a direct interaction of SOD with DNA. This was demonstrated by the fact that inactivated SOD displays inhibitory effects also.[69] However, this would argue against the results obtained with DTT present (Figure 3.14). Finally, in their study for active $Fe^{II}(BLM)$ intermediates, Rodriguez and Hecht have observed that when the concentration of SOD (or SOD mimics) is relatively high compared to the concentration of superoxide, inhibition effects are observed rather

than an increase in the DNA cleavage activity.[70] They propose that the SOD can react directly with reactive iron bleomycin intermediates, although this argument is not supported by experimental evidence.

Similar studies with mechanistic probes have been reported for related non-heme iron complexes, such as $[Fe^{III}(BDPEA)(Cl)_2]$,[56] $[Fe^{II}(L_5^+)(Cl)]$,[57] and $[Fe^{III}(MPE)]$.[27] With $[Fe^{III}(BDPEA)(Cl)_2]$, both SOD and catalase have a high inhibitory effect on the reaction (up to 95%), when O_2 is used as terminal oxidant and a reductant is added. Both $[Fe^{II}(L_5^+)(Cl)]$ and $[Fe^{III}(MPE)]$ display reduced activity in the presence of SOD (30-40% inhibition) and catalase (80-100% inhibition) under similar conditions. This inhibition pattern corresponds to the inhibition pattern obtained for **1**/H_2O_2 (Figure 3.12). Indeed, hydrogen peroxide has been proposed as an important intermediate in the DNA oxidation by the aforementioned complexes, demonstrated by the complete inhibition of the reaction by catalase.

Under these conditions, thus with O_2/DTT, catalase does not affect the cleavage reaction when **1** was employed as catalyst, which is in contrast to the aforementioned results with related complexes. A key finding is that SOD increases the cleavage activity, whereas in the other studies only inhibition was observed with this enzyme. Based on these data, it is proposed that superoxide and not hydrogen peroxide or hydroxyl radicals are important reduced oxygen species in the mechanism for **1**/O_2/DTT.

When excess hydrogen peroxide was added as oxidant, in the absence of DTT, the activity was comparable to that of **1**/O_2/DTT (*cf.* Figure 3.13 and Figure 3.14, lanes 1). In the presence of reductant (DTT), a significantly higher activity was observed (Figure 3.15) These experiments suggest that the overall activity of the catalytic system is largely dominated by the presence of **1** in a low oxidation state (*i.e.* Fe^{II}(N4Py)) This would, in turn, explain the lower activity in the **1**/O_2/SOD system without reductant (Figure 3.12).

3.3.2 Spectroscopic studies

Various attempts were made to investigate the reaction under catalytic conditions by spectroscopic means to gain information about the actual iron complex during reaction, to further substantiate the aforementioned hypothesis. Although UV/Vis spectroscopy is a very powerful technique for the investigation of these complexes (see Chapter 6), the strong absorption of DNA at 260 nm is a problem. Application of NMR is restricted also, due to the low intensity of the proton absorptions of the paramagnetic $[Fe^{II}(N4Py)(H_2O)]^{2+}$ complex.[38]

X-band ESR under catalytic conditions did not provide information due to the low concentration of the complexes of interest (1.0 μM). Moreover, the relatively low salt concentration precluded the formation of a good glass, which is required for these studies. When the concentrations were increased (0.5 mM iron complex, 75 mM Tris-HCl buffer, 1.5 mM DNA in base pairs) no signal was observed at 77K, in the presence or absence of DTT (1 mM, 2 equivalents with respect to the catalyst). Addition of H_2O_2 (1 mM, 2 equivalents with respect to the catalyst) to the mixture resulted in the appearance of a signal at g = 4.26, which corresponds to a high spin iron(III) complex (Figure 3.17). Surprisingly, higher concentrations of H_2O_2 did not result in the formation of the low spin $[(N4Py)Fe^{III}(\eta^1\text{-}OOH)]^{2+}$ complex (with ESR signals at g = 2.17, 2.12 and 1.98).[23] Earlier studies have demonstrated that slow addition of nearly equimolar H_2O_2 to **1** in acetonitrile results in the formation of $[(N4Py)Fe^{III}\text{-}OH]^{2+}$ and $[(N4Py)_2(Fe^{III})_2(O_2)]^{4+}$, whereas excess H_2O_2 results in the formation of the low spin $[(N4Py)Fe^{III}(\eta^1\text{-}OOH)]^{1+}$.[25] It should be mentioned here that these studies were performed in organic solvents.

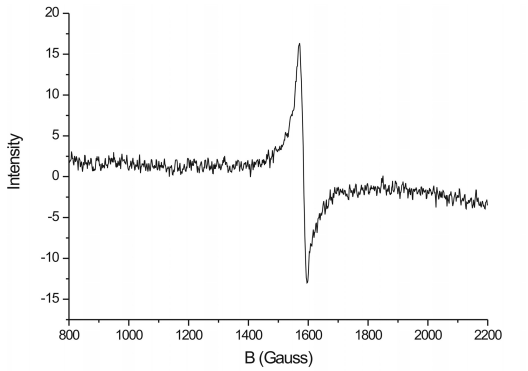

Figure 3.17 X-band ESR of **1** (0.5 mM) with salmon testes (ST) DNA (1.5 mM in base pairs) in Tris buffer (75 mM, pH = 8.0) with 1.0 mM H_2O_2 (2 equiv).

The absence of these ESR signals at 77K when DTT was employed and no H_2O_2 is present, suggests that the majority of the complex is in a reduced iron(II) state (which is ESR silent). Together with the results of the DNA cleavage experiments (Figure 3.14), it can be concluded that reduction of Fe^{III}(N4Py) back to Fe^{II}(N4Py) is of great importance for oxygen activation and thus efficient DNA oxidation.

3.4 Summary and conclusions

In this chapter, the oxidation of DNA by two mononuclear non-heme iron complexes was examined. The Fe^{II}(N4Py) complex (**1**) is capable of inducing strand cuts in the DNA solely via a single strand cleavage pathway. Pseudo-first order kinetics could be applied and a k_{obs} ~ 0.1 min^{-1} was determined via two methods: i) directly, by plotting -ln(f_l) against time and determining the resulting slope of the graph (Figure 3.10) and ii) indirectly, by calculating the average number of strand cuts from each sample, and subsequentially plotting these results as a function of time (Figure 3.11). The covalent attachment of an acridine moiety (complex **2**) improved the reaction constant by a factor of 4 (k_{obs} ~ 0.38 min^{-1}), but did not alter the reaction pathway, as only single strand cleavage was observed.

The reaction is dominated by the formation of reduced oxygen species, in particular superoxide radicals. It is likely that these superoxide radicals react with the iron complex to form iron intermediates in a higher oxidation state, rather than that the superoxide itself is involved in the hydrogen abstraction process. X-band ESR suggests the formation of a Fe^{III}(N4Py) species when H_2O_2 is added (g = 4.26). The absence of this ESR signal under aerobic conditions in the presence or absence of reductant makes it plausible that the majority of the complex is in a reduced state. Moreover, the absence of the typical ESR signals of the (N4Py)Fe^{III}OOH species (g = 2.17, 2.12 and 1.98) when excess H_2O_2 was added, seem to suggest an active involvement of DNA in the formation of certain intermediates. The drop in reactivity, when the DNA oxidation reaction was performed in a phosphate buffer, also suggests an interaction between the catalyst and phosphate moieties.

Based on the results of the inhibition experiments together with the limited spectroscopic information, a working hypothesis can be proposed (Scheme 3.5).

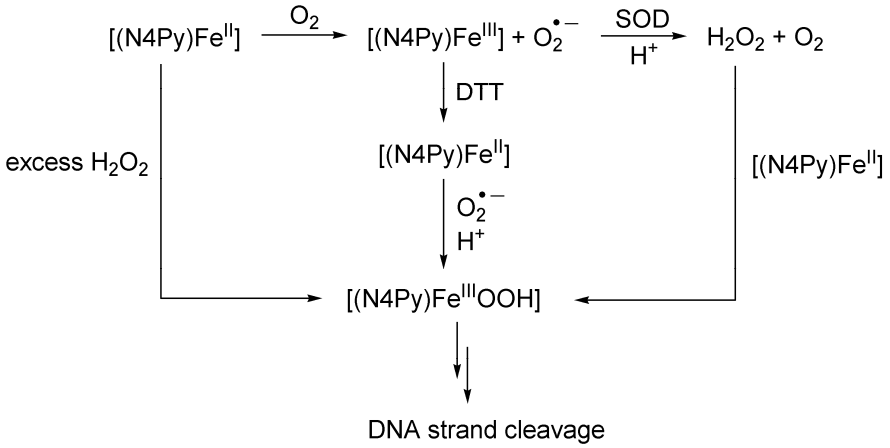

Scheme 3.5 Hypothesis for the activation of dioxygen by **1** to initiate oxidative DNA cleavage.

In this hypothesis, molecular dioxygen is activated to a superoxide radical, which in turn can react with a reduced iron complex, to form either $[(N4Py)Fe^{III}(\eta^2\text{-}O_2)]^+$ or $[(N4Py)Fe^{III}(\eta^1\text{-}OOH)]^{2+}$. The latter can be the actual hydrogen abstracting species for the DNA or a precursor for another species (*e.g.* $[(N4Py)Fe^{IV}{=}O]^{2+}$). Since the addition of catalase has no effect on the reaction, the formation of hydrogen peroxide as an alternative oxidant to dioxygen can be excluded. The addition of the hydroxyl radical scavenger DMSO to the reaction mixture did not influence the cleavage activity. This suggests a minimal role for hydroxyl radicals as alternative hydrogen abstracting species.

In conclusion, the Fe^{II}(N4Py) complex and its derivatives can induce DNA strand breaks at nanomolar concentrations. A central role is proposed for superoxide radicals in the catalytic cycle, which, in turn, can react with an iron complex in a low oxidation state. This might be a precursor for a metal complex in a high oxidation state (such as $(N4Py)Fe^{III}OOH$ or $(N4Py)Fe^{IV}{=}O$), which are responsible for the actual hydrogen abstracting from the DNA strand. However, more thorough (spectroscopic) studies are required to further substantiate this hypothesis.

3.5 Experimental Section

For general remarks on biochemical studies, see Chapter 2. Two methods of analyzing the agarose gel slabs was were used interchangably. Pictures of gel slabs were taken with a Spot Insight CCD camera, together with the software program Spot (version 3.4). The bands on the film were quantified using the software program Gel-Pro Analyzer version 4.0.00.001. However, the data in Figure 3.7a were collected using the method described in Chapter 2. The contrast of the pictures of the agarose slab gels, used as illustrations in this chapter, is inverted for clarity.

$[Fe^{II}(N4Py)(CH_3CN)](ClO_4)_2$ (**1**)[23] and $[(N4Py\text{-acridine})Fe^{II}(CH_3CN)](ClO_4)_3$ (**2**)[30] were synthesized according to literature procedures. Superoxide dismutase (SOD, from bovine erythrocytes) was purchased from Fluka, catalase (from bovine liver) was purchased from Sigma-Aldrich, and bovine serum albimum (BSA) was purchased from New England Biolabs. The activities of SOD[71] and catalase[72] are denoted in units (U). Other chemicals were purchased from Sigma-Aldrich, Acros, Lancaster, Fluka or Merck and used as received.

Caution: Perchlorate salts are potentially explosive and should be handled with care!

DNA oxidation reactions

A solution of **1** or **2** in H_2O and a solution of dithiothreitol (DTT) were added simultaneously to a buffered solution (Tris-HCl, 10 mM, pH = 8.0) of supercoiled pUC18 plasmid DNA (0.1 μg/μL; 150 μM in base pairs) to give a final concentration of 1.0 μM complex and 1.0 mM reductant. The mixture with a final volume of 50 μl was incubated at 37°C. At the times indicated, a sample (2 μL) was taken from the reaction mixture, diluted in 15 μL water (containing 1000 equiv of NaCN) and 3 μL loading buffer and frozen in liquid nitrogen immediately. Results are the average of three independent runs.

DNA oxidation in the presence of additives

When additives were used, they were added to the buffered DNA solution prior to the addition of the complex and reductant. The total volume of the reaction mixture was 25 μL. A sample was drawn from the solution after 30 min of incubation at 37°C, and quenched as described above. Results are the average of three independent runs.

Calculation of the uncertainty in the values by a Monte Carlo method

The uncertainty in the values of *n* and *m* were calculated with a Monte Carlo simulation using the software program Mathematica version 5.2.0.0. An algorithm was used, which calculated the results of both *n* and *m* from 5000 pseudo-random generated fractions sizes of supercoiled, nicked and linear DNA using Equations 3.1, 3.2, 3.5 and 3.6. These pseudo-random generated fractions sizes are based on the experimentally obtained average value (based on three independent runs) and generated within a normal distribution based on a standard deviation of 0.03. This standard deviation was determined independently by 24 identical DNA oxidation experiments with supercoiled pUC18 plasmid DNA and Fe(N4Py) (*vide supra*, reaction quenched at T = 30 min) and is the largest standard deviation observed in the experiment. Dr. R.M. Scheek is acknowledged for his help with the development of this Monte Carlo method, which is used throughout this thesis for the calculation of the uncertainty limits in the values of *n* and *m*.

Electron spin resonance (ESR) spectroscopic studies

Samples for measurement were transferred from the reaction solution to an ESR tube and were frozen in liquid nitrogen immediately. ESR spectra (X-band, 9.46 GHz) were recorded in liquid nitrogen (77 K) on a Bruker ECS 106 instrument, equipped with a Bruker ECS 041 XK microwave bridge and a Bruker ECS 080 magnet.

3.6 References and notes

1 See Appendix for abbreviations used.

2 *Bleomycin; Current Status and New Developments*, Eds.: S.K. Carter, S.T. Crooke, H. Umezawa, Academic Press, New York **1978**.

3 H. Umezawa, in: *Anticancer Agents Based on Natural Product Models*, Eds.: J.M. Cassady, J.D. Douros, Academic Press, New York **1980**, pp. 147-166.

4 S.M. Hecht, in: *Cancer Chemotherapeutic Agents*, Ed.: W.O. Foye, American Chemical Society, Washington D.C. **1995**, pp. 369-388.

5 J.S. Lazo, B.A. Chabner, in: *Cancer Chemotherapy and Biotherapy; Principles and Practice*, 2nd ed., Eds.: B.A. Chabner, D.L. Longo, Lippincott-Raven Publishers, Philadelphia **1996**, pp. 379-394.

6 J. Chen, J. Stubbe, *Nat. Rev. Cancer* **2005**, *5*, 102-112.

[7] U. Galm, M.H. Hager, S.G. Van Lanen, J. Ju, J.S. Thorson, B. Shen, *Chem. Rev.* **2005**, *105*, 739-758.

[8] *Bleomycin; Chemical, Biochemical and Biological Aspects*, Ed.: S.M. Hecht, Springer-Verlag, New York **1979**.

[9] S.M. Hecht, *Acc. Chem. Res.* **1986**, *19*, 383-391.

[10] J. Stubbe, J.W. Kozarich, *Chem. Rev.* **1987**, *87*, 1107-1136.

[11] J. Stubbe, J.W. Kozarich, W. Wu, D.E. Vanderwall, *Acc. Chem. Res.* **1996**, *29*, 322-330.

[12] R.M. Burger, *Chem. Rev.* **1998**, *98*, 1153-1169.

[13] S.M. Hecht, *J. Nat. Prod.* **2000**, *63*, 158-168.

[14] J. Chen, J. Stubbe, *Curr. Opin. Chem. Biol.* **2004**, *8*, 175-181.

[15] D.S. Sigman, A. Mazumder, D.M. Perrin, *Chem. Rev.* **1993**, *93*, 2295-2316.

[16] G. Pratviel, J. Bernadou, B. Meunier, *Angew. Chem. Int. Ed.* **1995**, *34*, 746-769.

[17] G. Pratviel, J. Bernadou, B. Meunier, *Met. Ions Biol. Sys.* **1996**, *33*, 399-426.

[18] G. Pratviel, J. Bernadou, B. Meunier, in: *Advances in Inorganic Chemistry, Vol. 45*, Ed.: A.G. Sykes, Academic Press, San Diego **1998**, pp. 251-312.

[19] P. Wesenhagen, *Oxidative DNA Cleavage by Artificial Metallonucleases*, Colloquium, University of Groningen, **2005**.

[20] M. Pitié, C. Boldron, G. Pratviel, *Advances in Inorganic Chemistry, Vol. 58*, Eds.: R. van Eldik, J. Reedijk, Academic Press, San Diego **2006**, pp. 77-130.

[21] Q. Jiang, N. Xiao, P. Shi, Y. Zhu, Z. Guo, *Coord. Chem. Rev.* **2007**, *251*, 1951-1972.

[22] M. Lubben, *Model Systems for Iron and Copper Containing Oxygenases*, Ph.D. thesis, University of Groningen, **1994**.

[23] M. Lubben, A. Meetsma, E.C. Wilkinson, B. Feringa, L. Que, Jr., *Angew. Chem. Int. Ed. Engl.* **1995**, *34*, 1512-1514.

[24] J. Kaizer, E.J. Klinker, N.Y. Oh, J.-U. Rohde, W.J. Song, A. Stubna, J. Kim, E. Münck, W. Nam, L. Que, Jr., *J. Am. Chem. Soc.* **2004**, *126*, 472-473.

[25] G. Roelfes, *Models for Non-Heme Iron Containing Oxidation Enzymes*, Ph.D. thesis, University of Groningen, **2000**.

[26] D.L. Boger, H. Cai, *Angew. Chem. Int. Ed.* **1999**, *38*, 448-476.

[27] R.P. Hertzberg, P.B. Dervan, *J. Am. Chem. Soc.* **1982**, *104*, 313-315.

[28] M. Wirth, O. Buchardt, T. Koch, P.E. Nielsen, B. Nordén, *J. Am. Chem. Soc.* **1988**, *110*, 932-939.

[29] M. Searcey, S. McClean, B. Madden, L.P.G. Wakelin, *J. Chem. Soc., Perkin Trans. 2* **1997**, 523-532.

[30] G. Roelfes, M.E. Branum, L. Wang, L. Que, Jr., B.L. Feringa, *J. Am. Chem. Soc.* **2000**, *122*, 11517-11518.

[31] E.L.M. Wong, G.-S. Fang, C.-M. Che, N. Zhu, *Chem. Commun.* **2005**, 4578-4580.

[32] W.K. Pogozelski, T.D. Tullius, *Chem. Rev.* **1998**, *98*, 1089-1107.

[33] R.P. Hertzberg, P.B. Dervan, *Biochemistry* **1984**, *23*, 3934-3945.

[34] N. Sträter, W.N. Lipscomb, T. Klabunde, B. Krebs, *Angew. Chem. Int. Ed. Engl.* **1996**, *35*, 2024-2055.

[35] E.L. Hegg, J.N. Burstyn, *Coord. Chem. Rev.* **1998**, *173*, 133-165.

[36] M. Komiyama, N. Takeda, H. Shigekawa, *Chem. Commun.* **1999**, 1443-1451.

[37] F. Mancin, P. Scrimin, P. Tecilla, U. Tonellato, *Chem. Commun.* **2005**, 2540-2548.

[38] W.R. Browne, R. Hage, *manuscript in preparation*.

[39] L.F. Povirk, W. Wübker, W. Köhnlein, F. Hutchinson, *Nucleic Acids Res.* **1977**, *4*, 3573-3580.

[40] D. Freifelder, B. Trumbo, *Biopolymers* **1969**, *7*, 681-693.

[41] H.J.C. Berendsen, *Goed Meten met Fouten*, Laboratorium voor Biofysische Chemie, Rijksuniversiteit Groningen, Groningen **1997**.

[42] A. Fersht, *Structure and Mechanism in Protein Science*, W.H. Freeman and Company, New York **1999**.

[43] P. Atkins, J. De Paula, *Atkins' Physical Chemistry*, 8th ed., W.H. Freeman and Company, New York **2006**.

[44] A. Decker, M.S. Chow, J.N. Kemsley, N. Lehnert, E.I. Solomon, *J. Am. Chem. Soc.* **2006**, *128*, 4719-4733.

[45] W.K. Pogozelski, T.J. McNeese, T.D. Tullius, *J. Am. Chem. Soc.* **1995**, *117*, 6428-6433.

[46] B.B. Keele, Jr., J.M. McCord, I. Fridovic, *J. Biol. Chem.* **1970**, *245*, 6176-6181.

[47] J.M. McCord, I. Fridovic, *J. Biol. Chem.* **1969**, *244*, 6056-6063.

[48] J.M. McCord, I. Fridovic, *J. Biol. Chem.* **1969**, *244*, 6049-6055.

[49] M.S. Lah, M.M. Dixon, K.A. Pattridge, W.C. Stallings, J.A. Fee, M.L. Ludwig, *Biochemistry* **1995**, *34*, 1646-1660.

[50] C.K. Vance, A.-F. Miller, *J. Am. Chem. Soc.* **1998**, *120*, 461-467.

[51] C.K. Vance, A.-F. Miller, *Biochemistry* **2001**, *40*, 13079-13087.

[52] G.C. Dismukes, *Chem. Rev.* **1996**, *96*, 2909-2926.

[53] A.J. Wu, J.E. Penner-Hahn, V.L. Pecoraro, *Chem. Rev.* **2004**, *104*, 903-938.

[54] J.W. de Boer, W.R. Browne, B.L. Feringa, R. Hage, *C. R. Chimie* **2007**, *10*, 341-354.

[55] J.E. Repine, O.W. Pfenninger, D.W. Talmage, E.M. Berger, D.E. Pettijohn, *Proc. Natl. Acad. Sci. U.S.A.* **1981**, *78*, 1001-1003.

[56] C. Hemmert, M. Pitié, M. Renz, H. Gornitzka, S. Soulet, B. Meunier, *J. Biol. Inorg. Chem.* **2001**, *6*, 14-22.

[57] P. Mialane, A. Nivorojkine, G. Pratviel, L. Azéma, M. Slany, F. Godde, A. Simaan, F. Banse, T. Kargar-Grisel, G. Bouchoux, J. Sainton, O. Horner, J. Guilhem, L. Tchertanova, B. Meunier, J.-J. Girerd, *Inorg. Chem.* **1999**, *38*, 1085-1092.

[58] C.J. Burrows, J.G. Muller, *Chem. Rev.* **1998**, *98*, 1109-1151.

[59] G. Scholes, R.L. Willson, M. Ebert, *J. Chem. Soc., Chem. Commun.* **1969**, 17-18.

[60] H.J.H. Fenton, *J. Chem. Soc.* **1894**, *65*, 899-910.

[61] S.A. Lesko, R.J. Lorentzen, P.O.P. Ts'o, *Biochemistry* **1980**, *19*, 3023-3028.

[62] E.J. Nanni, Jr., D.T. Sawyer, *J. Am. Chem. Soc.* **1980**, *102*, 7591-7593.

[63] D.T. Sawyer, J.S. Valentine, *Acc. Chem. Res.* **1981**, *14*, 393-400.

[64] J.M. Gebicki, B.H.J. Bielski, *J. Am. Chem. Soc.* **1981**, *103*, 7020-7022.

[65] B.H.J. Bielski, *Photochem. Photobiol.* **1978**, *28*, 645-649.

[66] G.J. McClune, J.A. Fee, G.A. McCluskey, J.T. Groves, *J. Am. Chem. Soc.* **1977**, *99*, 5220-5222.

[67] C. Bull, G.J. McClune, J.A. Fee, *J. Am. Chem. Soc.* **1983**, *105*, 5290-5300.

[68] G. Roelfes, V. Vrajmasu, K. Chen, R.Y.N. Ho, J.-U. Rohde, C. Zondervan, R.M. la Crois, E.P. Schudde, M. Lutz, A.L. Spek, R. Hage, B.L. Feringa, E. Münck, L. Que, Jr., *Inorg. Chem.* **2003**, *42*, 2639-2653.

[69] L. Galvan, C.-H. Huang, A.W. Prestayko, J.T. Stout, J.E. Evans, S.T. Crooke, *Cancer Res.* **1981**, *41*, 5103-5106.

[70] L.O. Rodriguez, S.M. Hecht, *Biochem. Biophys. Res. Commun.* **1982**, *104*, 1470-1476.

[71] One unit (1 U) of SOD corresponds to the amount of enzyme, which inhibits the auto-oxidation of pyrogallol by 50% at pH 8.2 and 25°C.

[72] One unit (1 U) of catalase will decompose 1.0 μmole of H_2O_2 per min at pH 7.0 at 25°C, while the H_2O_2 concentration falls from 10.3 to 9.2 mM, measured by the rate of decrease of A_{240}.